Journal of Electroceramics 5:3, 261–272, 2000

Synthesis of NASICON with New Compositions for Electrochemical Carbon Dioxide Sensors*

ENRICO TRAVERSA
Dipartimento di Scienze e Tecnologie Chimiche, Università di Roma ''Tor Vergata'', Via della Ricerca Scientifica, 00133 Roma, Italy

LAURA MONTANARO
Dipartimento di Scienza dei Materiali e Ingegneria Chimica, Politecnico di Torino, Corso Duca degli Abruzzi 24, 10129 Torino, Italy

HIROMICHI AONO & YOSHIHIKO SADAOKA
Department of Materials Science and Engineering, Faculty of Engineering, Ehime University, Bunkyo-cho, Matsuyama 790–8577, Japan

Submitted March 12, 1999; Revised May 3, 2000; Accepted June 6, 2000

Abstract. Powders and pellets of new NASICON compositions have been synthesized using a mixed inorganic-organic sol-gel synthesis, by the preliminary formation of a pre-hydrolized TEOS xerogel. The investigated compositions can be described by the general formula $Na_3Zr_{2-(x/4)}Si_{2-x}P_{1+x}O_{12}$, obtained by keeping the Na concentration constant $(=3)$ at the optimum value reported for ionic conductivity, with $x = 0$ (the usual NASICON composition), 0.667, and 1.333. The xerogels were calcined at various temperatures in the range 400–1200°C. The powder samples were analyzed by TG/DTA, BET measurements, XRD, and SEM. The powders calcined at 500°C were sintered into pellets at 1100°C for 6 h. The sintering behavior of the pellets was investigated by dilatometric measurements and SEM observations. The sinterability increased with increasing x value. Dense samples of the new compositions were obtained by sintering at only 1100°C. This is attributed to the occurrence of liquid phase sintering. The electrical conductivity of the NASICON sintered bodies was measured by ac impedance spectroscopy. The conductivity decreased with decreasing c_0 lattice parameter of the hexagonal structure or increasing x value. The CO_2 gas sensors, using as electrolyte the dense samples of the new NASICON compositions, showed good EMF response that was very close to the theoretical value, even for the sample with $x = 1.333$ that showed much lower conductivity.

Keywords: NASICON, sol-gel, ionic conductors, electrical properties, solid electrolyte, CO_2 detection, electrochemical sensors

1. Introduction

The problem of global warming, associated with the increased level of carbon dioxide emitted in the atmosphere, needs the development of low-cost CO_2 detection methods. For this purpose, potentiometric sensors using alkali-ion-conducting solid electrolyte are very promising being very selective to CO_2 [1–6]. The properties of NASICON are suitable for use in electrochemical devices, provided that the ceramic is dense. A commercial NASICON product (NGK Co. Ltd, Japan) with nominal composition $Na_3Zr_2Si_2PO_{12}$ was investigated as a CO_2 electrochemical sensor [7–9]. However, the porosity of the NASICON materials was too high to guarantee a sensing performance adequate for practical applications. One of the main challenges in the preparation of NASICON ceramics is the lowering of their sintering temperature [10]. Below

*Paper presented at the Italy–Japan Bilateral Seminar on Functional Ceramic Materials, held in Tokyo on September 29, 1998.

we summarize key characteristics of NASICON and attempts to fabricate high quality ceramics.

One of the first studies on NASICON was performed by Hong [11] who reported that solids in the composition range $Na_{1+x}Zr_2Si_xP_{3-x}O_{12}$, with $0 < x < 3$, crystallize in the NASICON structure when heated to 1200°C. This structure has a rhombohedral symmetry, except in the interval $1.8 < x < 2.2$, where a small distortion to monoclinic symmetry occurs. The structure of NASICON compounds is characterized by a three-dimensional framework of SiO_4 and PO_4 tetrahedra corners shared with ZrO_6 octahedra, in which Na^+ ions occupy the interstices [11]. Thus, these compounds present a Na^+ ionic conductivity comparable to that of β-alumina, which is characterized by a two-dimensional Na^+ ionic mobility.

NASICON-type structures exist in a large triangular portion of the quaternary phase diagram Na_2O-ZrO_2-P_2O_5-SiO_2, delimited by the compositions: $NaZr_2P_3O_{12}$, $Na_4Zr_2Si_3O_{12}$, and $Na_4Zr_{1.25}P_2O_{12}$ [12]. Nevertheless, most of the studies on NASICON have been concentrated on the above reported general formula, in the composition range $1.8 < x < 2.4$ [13–17], because the compounds in that range showed the highest conductivity values [18,19]. Only few investigations were devoted to different compositions [12,20–24]: Kohler et al. [12] and later Rudolf et al. [21,22] succeeded in preparing Zr-deficient monoclinic compositions. Outside the aforesaid triangular portion of the phase diagram, metastable NASICON phases were also synthesized [25].

The synthesis of NASICON as a pure phase is very difficult, especially when performed by solid-state reaction [15,26,27]. The NASICON phase can be accompanied by formation of zirconia and a glassy phase [28]. In order to obtain zirconia-free materials, Von Alpen et al. [29] proposed a different general formula: $Na_{1+x}Zr_{2-x/3}Si_xP_{3-x}O_{12-2x/3}$. However, though zirconia-free, the materials with this formula also consisted of two phases [30]. The formation of a glassy phase (which is basically a sodium silicophosphate with some dissolved zirconia [28]) has been ascertained for many compositions, [24,28,30] mostly in the silica-rich side. The glassy phase has a large ionic conductivity, but it is rapidly degraded upon contact with water. Moreover, new, liquid phases were formed after high temperature treatments, which were found to improve the powder sinterability [28,30,31].

Different chemical routes for obtaining pure NASICON phases have been investigated, such as wet chemical processes [13,14], combustion synthesis, [32] hydrothermal [33] and sol-gel techniques [16,34–39]. Solution syntheses offer more homogeneous materials; the higher reactivity of the precursors could lead to purer phases and small grains with improved sinterability [24]. Generally, the crystallization of the amorphous precursors lead directly to the hexagonal structure of NASICON, using wet-chemical routes [15,16]. On the other hand, this structure is stable only at temperatures higher than 200–300°C when it is formed from the monoclinic structure yielded by the solid-state reactions [13]. However, the orientational disorder, which is derived by the processing and thermal history of NASICON, affects the rhombohedral to monoclinic phase transition for NASICON [40].

The first sol-gel synthesis of NASICON dates back to 1983 [16], and since then the gel syntheses of NASICON ceramics have been extensively explored [41,42]. However, the preparation of pure NASICON by sol-gel starting from all organic precursors is somewhat problematic, [24,43] while the use of inorganic precursors in aqueous solutions produced NASICON powders of improved quality [44].

Recently, the authors of this paper proposed the synthesis of new NASICON compositions in order to improve its sinterability [45]. In particular, we selected compositions in the $Na_3Zr_{2-(x/4)}Si_{2-x}P_{1+x}O_{12}$ range, thus keeping the Na concentration constant $(= 3)$ at the optimum value reported for ionic conductivity. The materials were prepared using a mixed inorganic-organic sol-gel synthesis, reported in the literature for the preparation of other heterometallic oxides [46,47].

For these new NASICON compositions, the correlation between the phase, the sinterability, the microstructural evolution during the sintering, and the electrical conductivity is reported in this paper. Given that a direct relationship between conductivity and the size of the c parameter in the hexagonal cell has been clearly established [20], the resulting modifications of the cell parameters as a function of the composition were especially studied. Finally, pellets made with the NASICON powders with the new compositions were tested in CO_2 gas sensors and their sensing performance was correlated with the materials characteristics.

2. Experimental Procedure

2.1. Materials Preparation

NASICON-type materials in the $Na_3Zr_{2-(x/4)}Si_{2-x}P_{1+x}O_{12}$ system, with $x = 0$ (the standard NASICON composition, used as reference), 0.667, 1.333, and 2, labeled A, B, C, and D, respectively, were prepared. For sample B, in order to verify the structural and microstructural modifications induced by limited compositional changes, the Na content was changed slightly keeping the Zr content constant, in order to get a Na-excess ($Na_{3.2}Zr_{1.833}Si_{1.532}P_{1.467}O_{12}$, $B + 0.2$ sample) and a Na-deficient composition ($Na_{2.8}Zr_{1.833}Si_{1.132}P_{1.868}O_{12}$, $B - 0.2$ sample).

The powders were prepared using a mixed organic-inorganic sol-gel technique, which involved the preliminary formation of an amorphous solid (xerogel), by modifying the molar ratios between the metal-organic reagent, tetraethylortosilicate (TEOS), absolute ethanol (EtOH) and water, according to an improvement of a procedure previously reported [48]. A measured volume of TEOS was added to ethanol and distilled water in order to have a TEOS : EtOH : water molar ratio of 1 : 10 : 4. These values were chosen considering the TEOS-water-EtOH ternary phase diagram [49], in order to perform the synthesis in the miscible area of the diagram, and thus to better homogenize the reactants and to limit the segregation of zirconia.

The mixture was stirred for 30 min adjusting the pH at about 1–1.5 with the addition of a 1 M solution of HNO_3. Stoichiometric quantities of $NaNO_3$ and $ZrO(NO_3)_2$ were dissolved in water and added to the previous solution under stirring until a clear phase was obtained. After that, a suitable portion of $(NH_4)_2HPO_4$ aqueous solution was quickly added, always under stirring. A gelatinous precipitate appeared, which after about half an hour of stirring was dried at 105°C in an oven and then calcined in air for 30 min at various temperatures in the 400–1200°C range.

The powders were then ground in a planetary mill for 4 h in absolute ethanol to obtain a narrow particle size distribution, lower than 5 μm, as confirmed by laser granulometry (Malvern Particle Sizer 3600D).

The powders calcined at 500°C were uniaxially (150 MPa) and then isostatically (200 MPa) pressed into pellets of 10 mm in diameter, and sintered at 1100°C for 6 h. Sintering at 1100°C was performed in order to control the loss of Na during the heat treatments, even though this temperature is lower than the sintering temperatures usually reported by other authors [50].

2.2. Measurements on Materials

The dried powders were analysed by simultaneous thermogravimetric and differential thermal analysis (TG-DTA, Netzsch mod. STA 409, with a heating rate of 10°C/min in flowing air), in order to determine the crystallization temperature of the xerogels.

The phase evolution of the powders was analyzed by X-ray diffraction (XRD, CuKα radiation, $\lambda = 1.54060$ Å), after calcination at different temperatures. The XRD patterns were recorded at room temperature (20°C) with a Philips PW1710 diffractometer equipped with a graphite monochromator in the diffracted beam and a sample spinner (40 kV, 25 mA, 0.01 θ step, 5 s counting time). The lattice parameters, the cell volume and the corresponding theoretical density were determined as a function of composition, as reported in detail elsewhere [51]. The changes in the specific surface area after calcination at various temperatures were investigated by nitrogen adsorption.

The sintering behavior of the pellets was investigated by dilatometric measurements (Netzsch 402E Dilatometer; heating and cooling rate of 5°C/min, isothermal step of 6 h at the max temperature of 1100°C). The final densities were evaluated by geometrical measurements and weight determination.

The microstructure of the powders (as a function of composition and thermal treatments) and of the sintered materials was observed by scanning electron microscope (SEM, JEOL mod. JSM-5310).

For the electrical conductivity measurements, Au electrodes were deposited by sputtering on both sides of the NASICON pellets. The electrical conductivity of the pellets was determined by means of ac impedance spectroscopy measurements, performed as a function of the temperature in the frequency range 100 Hz to 10 MHz.

2.3. CO_2 Gas Sensing Measurements

Figure 1 shows the structure of the sensor probe. Each NASICON disk tested was fixed at the end of an alumina tube with an inorganic adhesive. A platinum

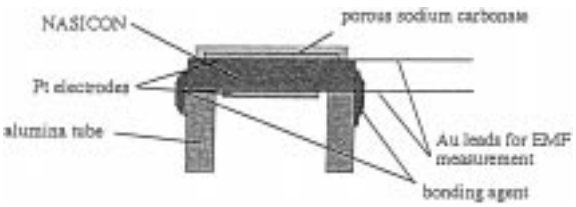

Fig. 1. Structure of the sensor probe.

electrode was painted onto both sides of the NASICON disks and then heated to 800°C. The Pt electrode on the pellet inside the tube acted as a reference electrode. A porous Na_2CO_3 layer on the measuring platinum electrode was used as auxiliary electrode. For its preparation, a saturated Na_2CO_3 solution was dripped on the Pt electrode on the outside face and then dried at 80°C. The as-prepared element was set in a quartz chamber of 20 ml in volume. For the reference electrode, ambient air was introduced inside the alumina tube at a flow rate of 100 ml/min. A controlled flow, at a flow rate of 100 ml/min, of artificial air ($CO < 1$ ppm, $CO_2 < 2$ ppm, $HCl <$ 1 ppm, and $H_2O < 10$ ppm), without or with CO_2 at 10, 100, 1000, and 10,000 ppm concentrations, was introduced in the chamber in contact with the sensing electrode side. The EMF of the sensor was measured using a digital electrometer.

3. Results and Discussion

3.1. Powder Analysis

The TG-DTA curves for the samples tested showed a large weight loss (about 40 wt %) in two steps, attributed to the loss of adsorbed water and to the oxidative decomposition of the organic chains (between 300°C and 500°C, accompanied by an exothermic effect), respectively. A broad DTA peak was observed in the temperature range 650°C–800°C, which might be associated with NASICON crystallization [14]. The presence of two overlapping peaks was observed at the same temperature range only for sample D.

Given the TG-DTA results, the NASICON powders started their crystallization around 700°C. The XRD patterns of the samples heated at the as-determined crystallization temperatures showed only broad peaks of the NASICON structure. The powders were calcined at 900°C and 1200°C for 30 min to obtain well crystallized samples. All the products heated to 900°C showed broad peaks of the NASICON structure and were free of zirconia peaks. After calcination at 1200°C, all the compositions but D were free from foreign phases, such as zirconia. The NASICON structure presented a monoclinic symmetry for composition A and a rhombohedral symmetry for all the others. The sample D was formed by a mixture of two phases: $Na_2ZrP_2O_8$ [52], and a hexagonal NASICON phase. For this reason, we did not consider sample D for further investigations.

The XRD data for the NASICON samples are summarized in Table 1. A significant evolution of the cell parameters and volume was found as a function of the composition. It has been previously reported that a continuous reduction of the cell parameters was measured with decreasing zirconium and silicon content [51], and the same trend was observed for the samples studied in this work. For samples B and C, the Na molar content in the formula was kept constant and equal to the value of sample A, the reference NASICON, while their composition evolved with a progressive decrease in the Zr and Si molar contents. The cell parameters and related cell volume are expected to decrease with a reduction of Zr and Si ions. In fact, given that the principal building units of the characteristic NASICON three-dimensional network are ZrO_6 octahedra with corners shared by $(Si,P)O_4$ tetrahedra [11,12], a lower Zr composition has a significant influence in reducing the cell dimension.

The Zr ion content in the formula is constant for samples B, B + 0.2, and B − 0.2. For the classical NASICON composition, $Na_{1+x}Zr_2Si_xP_{3-x}O_{12}$, it has been reported that an increase in the x value, which means the substitution of the larger Si ions for P ions and associated insertion of charge-compensating Na ions, causes the a_0 axis to increase monotonically, while the c_0 parameter rises up to a maximum at $x = 2$ and then decreases [53]. A similar relationship was found for the cell parameters of the NASICON samples B, B + 0.2, and B − 0.2, as shown in Fig. 2, which reports the changes in a_0 and c_0 cell parameters as a function of the Na content for the present compositions in the B-series and the classical NASICON composition with $1.8 < x < 2.2$ (data from [53]). The a_0 and c_0 parameters for classical NASICON were evaluated considering a pseudo-hexagonal cell starting from the data of the

Table 1. X-ray Diffraction data for NASICON powder samples crystallized at 1200°C for 30 min

Sample	Composition	Symmetry	Cell parameters (Å)	Cell volume (Å^3)
A	$Na_3Zr_2Si_2PO_{12}$	Monoclinic	$a_0 = 15.589$ $b_0 = 9.03$ $c_0 = 9.224$ $\beta = 124.09°$	
B	$Na_3Zr_{1.833}Si_{1.333}P_{1.677}O_{12}$	Rhombohedral	$a_0 = 8.951$ $c_0 = 22.990$	1588.900
B + 0.2	$Na_{3.2}Zr_{1.833}Si_{1.532}P_{1.467}O_{12}$	Rhombohedral	$a_0 = 8.990$ $c_0 = 22.972$	1607.815
B − 0.2	$Na_{2.8}Zr_{1.833}Si_{1.132}P_{1.868}O_{12}$	Rhombohedral	$a_0 = 8.925$ $c_0 = 22.952$	1583.270
C	$Na_3Zr_{1.667}Si_{0.667}P_{2.333}O_{12}$	Rhombohedral	$a_0 = 8.894$ $c_0 = 22.908$	1569.276
D	$Na_3Zr_{1.5}P_3O_{12}$	Rhombohedral	$a_0 = 8.82$ $c_0 = 22.79$	
	$Na_2ZrP_2O_8$	Card 35–0125		

monoclinic structure [20]. The variation of the a_0 parameter has a more significant influence on the cell volume, which monotonically increases with an increase in the Na content. The room-temperature c_0 parameter values for the new compositions are larger than those for the classical NASICON, being closer to those shown by $Na_3Zr_2Si_2PO_{12}$ at higher temperatures (22.980 Å at 170°C and 23.057 Å at 350°C [53]).

Higher specific surface area (SSA) were measured for the samples richer in Si, at lower calcination temperatures. However, the SSA strongly decreased for the Si-rich samples with increasing temperature and approaching their crystallization, while the SSA reduction was less sharp for powder C [45]. The decrease in SSA for the powder A was nearly concentrated between 400 and 500°C, which is the temperature range corresponding to the decomposition of the organic residues, as observed in the TG-DTA curve.

The above data allowed us to select 500°C as the more suitable calcination temperature of the powders, before forming and sintering; in fact, at this

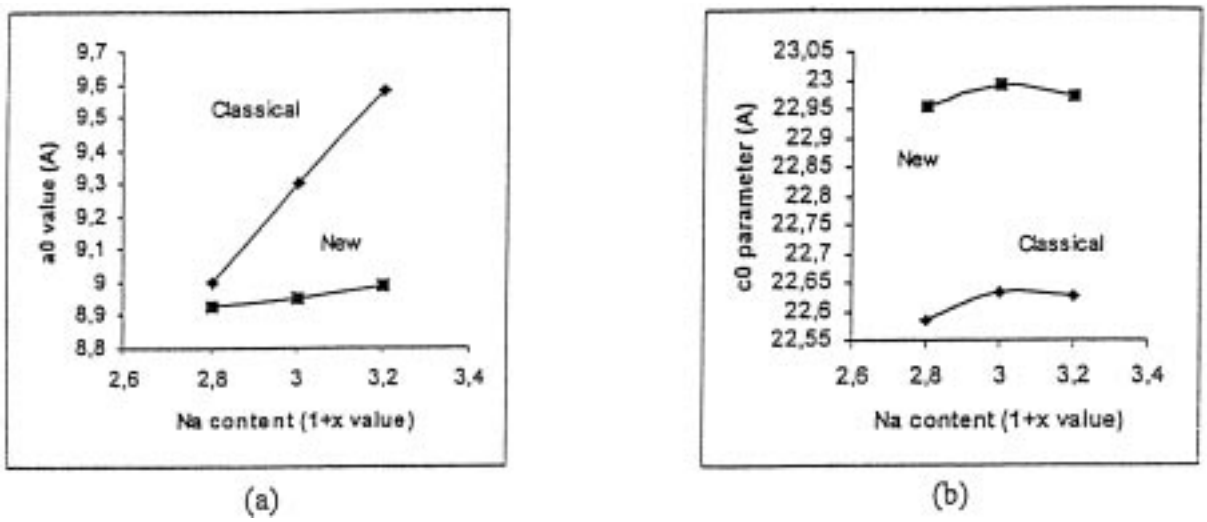

Fig. 2. Comparison between the changes in cell parameters as a function of the Na content for the classical NASICON ((a), data from Boilet et al. [53]) and new compositions in the B series (b).

temperature the weight loss of the precursors was almost completed. Thus, this temperature avoids large shrinkage during sintering induced by significant residual weight loss, but also keeps the powders reactive enough during densification. After calcination and milling, all the powders presented a similar, narrow particle size distribution, very close to the mean value of 5–6 μm, with an upper limit of about 15 μm.

3.2. NASICON Sinterability

Figure 3 shows the dilatometric curves during heating measured for the NASICON samples. Several dilatometric curves showed a slight contraction up to 100°C, followed by an expansion, as already reported in the literature for NASICON or NASICON-type materials [13,15,54]. Significant differences in sintering are evident; sample A underwent a single-step sintering process having an onset temperature of about 700°C. The total shrinkage was about 11% and it was almost completed at about 900°C. This process can be ascribed to crystallization of the NASICON powder, as determined by DTA, which is overlapped by the solid-state sintering of the reactive grains. The samples in the B-series showed a two-step sintering process, having an onset temperature of about 740°C and about 1000°C, respectively. The total shrinkage ranged between 15% for sample B and 23% for sample B − 0.2. The contribution of the two steps changed with the P content; the shrinkage associated with the lower temperature step become larger while the shrinkage at higher temperatures become smaller with decreasing the P content. A two-step sintering process, with onset temperatures at about 680°C and 950°C, was observed for sample C, although most of the shrinkage was associated with the step at higher temperature. This sample underwent a total shrinkage of about 25%.

Also in the A, B, and C series the influence of the second sintering step is larger with increasing P content. Thus, the second step of the sintering process is ascribable to liquid phase sintering, due to the formation of a glassy phase in the temperature range 950–1050°C. The high temperature liquid phase is formed due to the high content of glass-forming oxides, such as silica and phosphorous oxide [30]. In fact, the onset temperature of liquid phase formation decreased with increasing P content, being minimum (950°C) for sample C. These findings support the hypothesis already suggested in the literature [24,28,30,40] that NASICON undergoes liquid phase sintering.

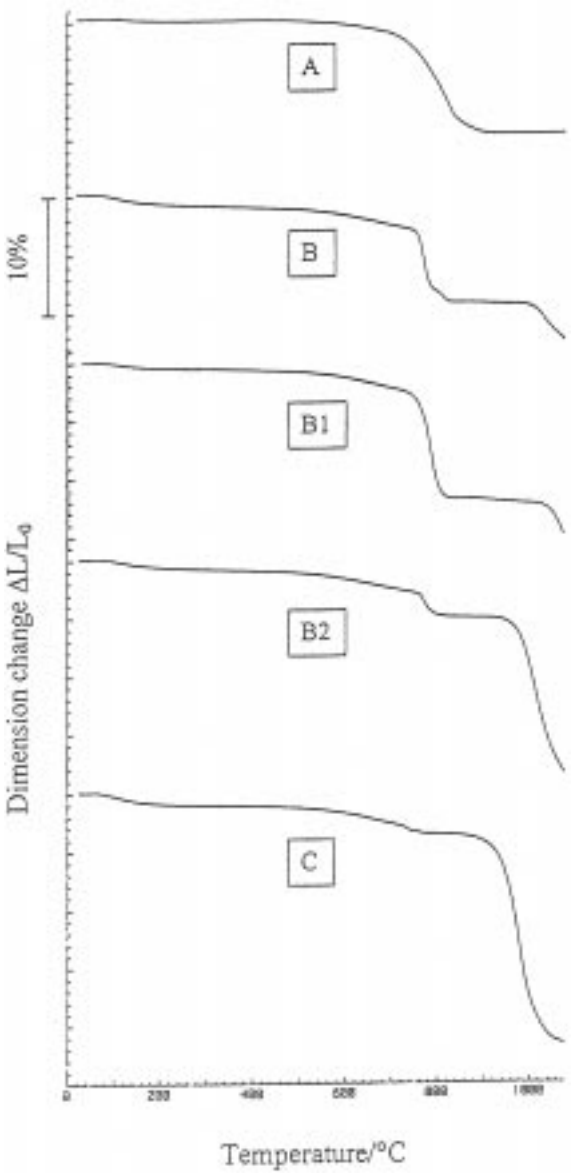

Fig. 3. Dilatometric curves on heating of the five NASICON compositions (A, B, B + 0.2, B − 0.2, and C, from top to bottom).

3.3. NASICON Pellet Analysis

Table 2 shows the final densities of the NASICON pellets. The density of the sample A sintered at 1100°C did not exceed 75% of the theoretical value

Table 2. Final density and phases present as obtained from XRD analysis for the NASICON pellets sintered at 1100°C for 6 h

Sample	Density (% theoretical value)	Phases present (from XRD analysis)
A	75	NASICON + tetragonal ZrO_2
B	92	NASICON
B + 0.2	92	NASICON
B − 0.2	88	NASICON + tetragonal ZrO_2
C	89	NASICON

(3.259 g/cm^3), even though the green density was large (about 55–65%). This confirmed the poor sinterability of the typical NASICON composition [24]. On the other hand, all the new NASICON materials showed a better densification, their density ranging between 88% and 92% of the theoretical value (3.196 g/cm^3). This good sinterability was obtained at a temperature which is lower than the sintering temperatures usually reported in the literature for NASICON materials [50]. Given that all the samples underwent the same type of processing and thermal histories, their different behavior should be attributed only to their different composition.

Results of XRD analysis for the pellets sintered at 1100°C made of the five NASICON compositions are also reported in Table 2. While a single NASICON phase was observed for the powders for all the compositions, the separation of a small amount of tetragonal zirconia was clearly observed for the A and B − 0.2 compositions.

Figure 4 shows the SEM micrographs of the surface for the pellets sintered at 1100°C made of the five NASICON compositions. Pellet A (Fig. 4(a)) showed the presence of large porosity. In the dense areas, relatively small grains (around 500 nm) seem to be embedded in a glassy phase. According to SEM observations, the low sinterability of composition A was due to the presence in the powder of hard agglomerates, which generated a structure with both dense and highly porous regions.

In agreement with the density measurements (Table 2), the presence of pores was hardly detected for the other pellets, while small cracks were observed for pellet C (Fig. 4(e)). SEM observations clearly showed the presence of a glassy phase on the surface of sample B, which makes the observation of the crystalline grains difficult (Fig. 4(b)). The morphology of pellet B + 0.2 was somewhat similar to that of pellet A, with a sharp reduction in porosity and an increase in the glassy phase amount (Fig. 4(c)). Sample B − 0.2 showed a homogeneous microstructure of micron-sized equiaxed grains, with a reduced amount of glassy phase (Fig. 4(d)). However, the more significant microstructural change was observed for pellet C, which showed a substantial amount of glassy phase embedding large (5 to 10 μm in size) and regularly-shaped grains, with a well-faceted appearance (Fig. 4(e)).

SEM observations of these samples clearly showed the presence of a glassy phase at the high sintering temperature, in agreement with the other findings reported above. The high temperature liquid or transitory viscous phase gave rise to a glassy phase on cooling. The appearance of this liquid phase may induce the segregation of zirconia crystals by a dissolution-precipitation process. The preferential growth of NASICON crystals is also ascribed to the presence of the glassy phase, observed for pellets C and B − 0.2, the richest in P. According to SEM observations, grain growth can again be favored by a dissolution-recrystallization mechanism in the liquid phase.

3.4. Electrical Conductivity

The electrical conductivity of the NASICON sintered bodies was measured by ac impedance spectroscopy, which in general allows one to distinguish the bulk and the grain boundary resistances in polycrystalline electrolytes [55]. A typical impedance spectra in the complex impedance plane for the NASICON pellets at all the temperatures tested showed the presence of a single semicircle at higher frequencies, together with a linear Warburg-like spike inclined at about 45° at lower frequencies. The behavior at low frequency can be ascribed to the electrolyte/electrode interface. The electrodes used were made of Au, an electron conductor, while the charge carriers in NASICON are Na^+ ions. The excess charge due to the charge build-up at the metal electrodes causes a polarization effect at the electrodes.

Since a single semicircle was observed in the impedance, this did not allow separation of the bulk and of the grain boundary contributions [56]. In this case, the values of total conductivity were evaluated from the complex impedance plane plots, calculated from the intercepts of the semicircle with the real axis.

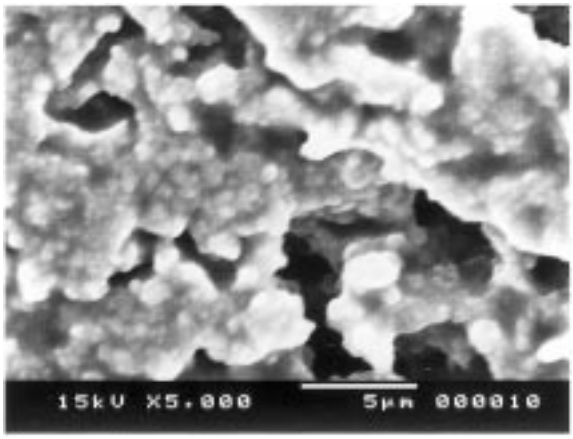

(a)

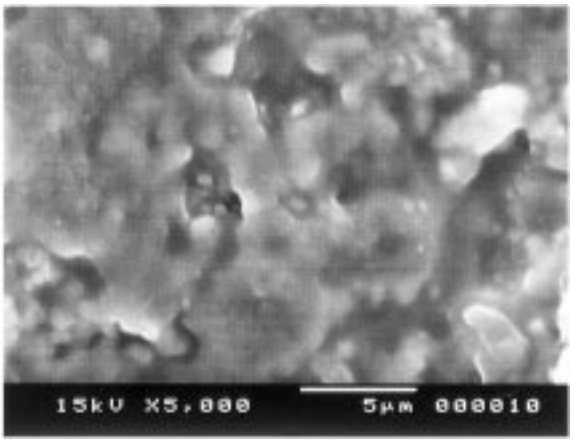

(b)

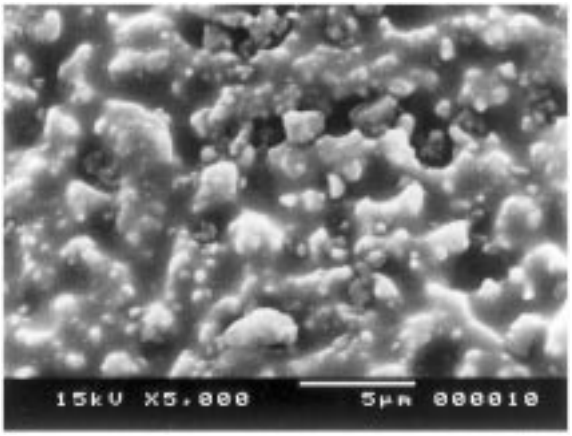

(c)

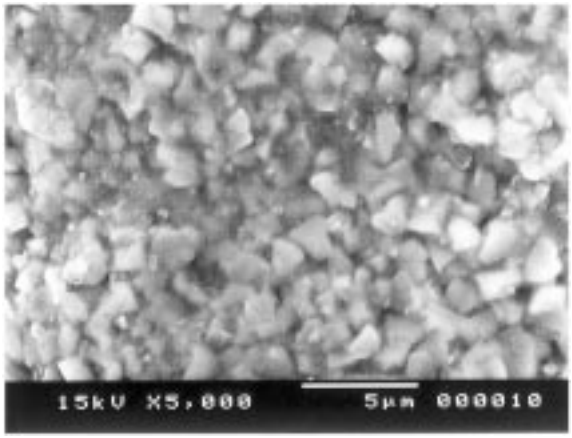

(d)

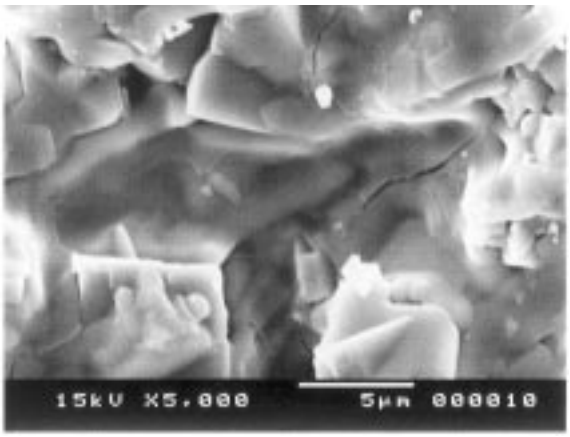

(e)

Fig. 4. SEM micrographs of the surface of the pellets sintered at 1100°C made of the five NASICON compositions, A (a), B (b), B + 0.2 (c), B − 0.2 (d), and C (e).

These values are attributed to a prevalent effect of bulk conductivity and thus will be discussed.

Figure 5 shows the temperature-dependence of the conductivity for the A, B, and C samples. The highest conductivity was shown by sample B at lower temperatures. It is known that the NASICON conductivity decreases with a decrease in the lattice constants because of a reduction of the tunnel size for Na^+ migration [20,56]. Thus, the larger conductivity should be expected for the sample A because it has larger lattice constants than the sample B. However, sample A was very porous, and the conductivity of the sample B, we believe, was increased with respect to sample A by its higher density.

A change in slope of the Arrhenius plots was observed for all samples at a temperature around 450–500K, as reported in the literature [10,28]. The change in slope indicates a change in the conduction mechanisms, which has been earlier correlated with a phase transition [40,57]. However, there is uncertainty in this attribution, as in the present case; in fact, a change from rhombohedral to monoclinic phase is possible for the NASICON structure with conventional $Na_3Zr_2Si_2PO_{12}$ composition, but phase changes were not observed for the other compositions.

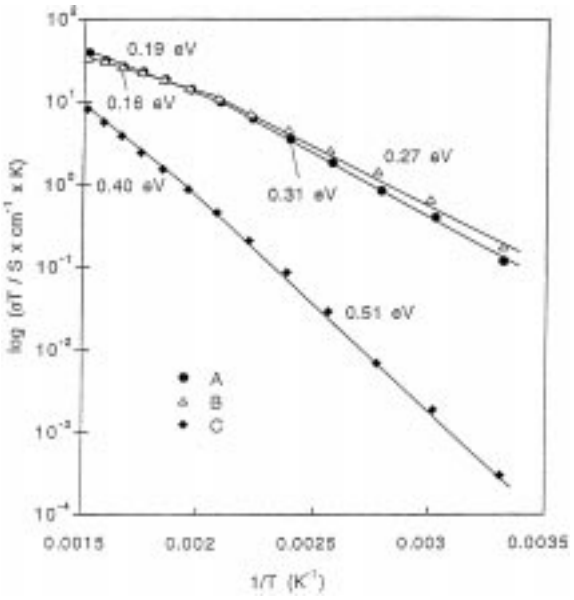

Fig. 5. The temperature-dependence of σT for the A, B, and C NASICON pellets, sintered at 1100°C.

For the case of NASICON phases having Li^+ ionic conduction, it has been reported that the change in the slope of the Arrhenius plot is due to the bulk conductivity, while at lower temperatures the conductivity through grain boundaries dominates (the activation energy for the bulk conductivity is lower than that for the grain boundary conductivity) [58,59]. However, in our case, the separation between bulk and grain boundary conductivity was not possible.

The calculated activation energies were 0.31 eV at low T and 0.19 eV at high T for sample A, and 0.27 eV at low T and 0.16 eV at high T for sample B. The measured conductivity and activation energy values are in line with the values reported in the literature for NASICON [40], although the sintering temperature was as low as 1100°C. On the other hand, the conductivity of the sample C was much lower and the activation energy for ion migration was much larger (0.51 eV at low T and 0.40 eV at high T). In this case, the smaller tunnel size strongly influenced the conductivity of sample C. Another explanation of the smaller conductivity of sample C is the presence of a larger amount of glassy phase, which should possess a lower conductivity than that of the NASICON phase [60].

Figure 6 shows the temperature-dependence of the conductivity for the B, B + 0.2, and B − 0.2 samples. The density of the three samples was nearly the same. The c_0 parameter goes in the order: B > B + 0.2 > B − 0.2. The activation energies at high and low temperatures increased in the opposite order: B < B + 0.2 < *B* − 0.2. At T < 450K, sample B showed larger conductivity, and the conductivity values observed for sample B + 0.2 were larger than those for sample B − 0.2, though very slightly. However, at higher temperatures the trend of conductivity was the opposite. This trend was not always reproducible, so that a correlation with the lattice parameters is uncertain.

3.5. *CO_2 Response*

For the CO_2 detection, the cell was prepared according to the equilibrium potential (type III) cell reported in Yamazoe and Miura [61]. The electrochemical cell was prepared combining NASICON as solid electrolyte with Na_2CO_3 as auxiliary phase. Therefore, the sensor consists in a half-cell that respond to CO_2 and a half-cell that is sensitive to O_2. The potential of the latter cell is kept constant by

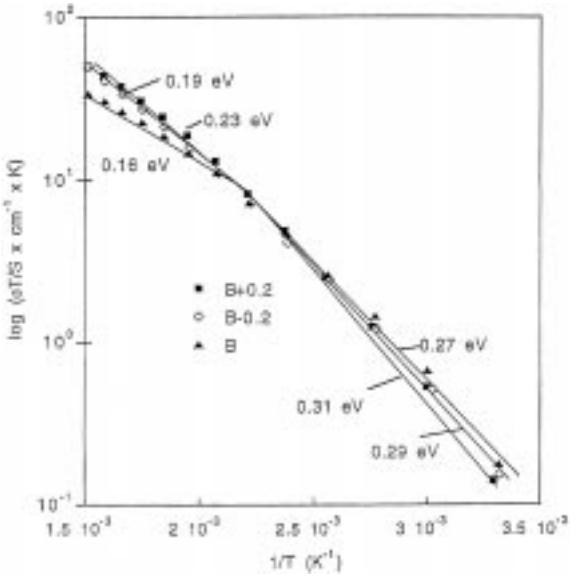

Fig. 6. The temperature-dependence of σT for the B, B + 0.2, and B − 0.2 NASICON pellets, sintered at 1100°C.

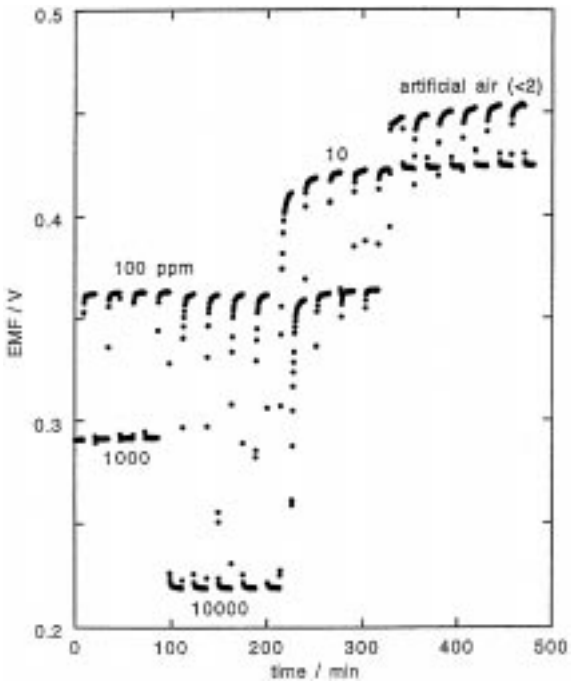

Fig. 7. The CO_2 sensing response at 470°C for the B NASICON pellet, at various CO_2 concentrations (ppm) shown in the figure.

exposing it to air. The electrode reactions are reported in Yamazoe and Miura [61].

Figures 7 and 8 show the EMF response to different concentrations of CO_2 for samples B and C, respectively, measured at 470°C. A stable EMF response with a good performance was obtained for both samples, also for the sample C which showed a lower conductivity. The response time, both in adsorption and desorption of CO_2, was very low especially at high CO_2 concentrations. Figure 9 shows the relationship between the EMF and the CO_2 gas concentration for the gas sensors prepared using the A, B, and C samples. The EMF values for the sensor using sample A were close to zero. The large porosity of this sample allowed the gas to flow through the electrolyte from the measuring electrode to the reference electrode. In the case of the sensor using the dense B or C electrolyte, the measured sensitivity of 72.5 mV/decade was in good agreement with the theoretical value of 74.0 mV/decade based on a two-electron electrochemical reaction [6].

These findings allow us to state that the dense NASICON electrolytes with new compositions, even though their conductivity is smaller than the conductivity of the classical NASICON composition, are promising for the application as solid electrolyte in

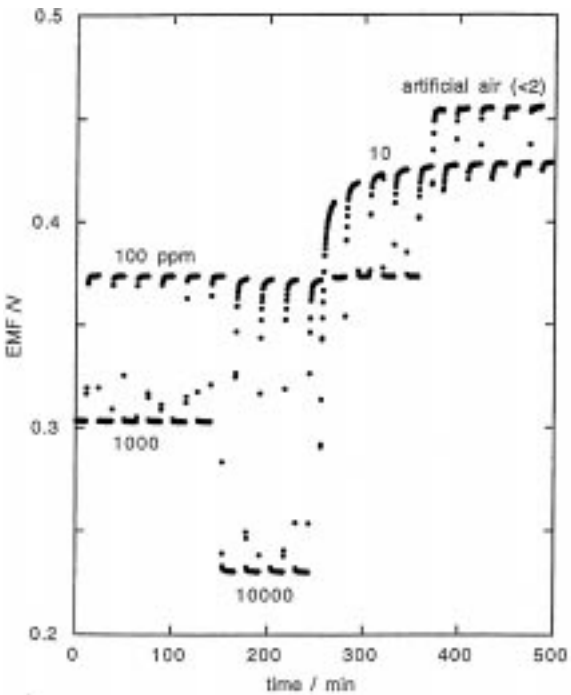

Fig. 8. The CO_2 sensing response at 470°C for the C NASICON pellet, at various CO_2 concentrations (ppm) shown in the figure.

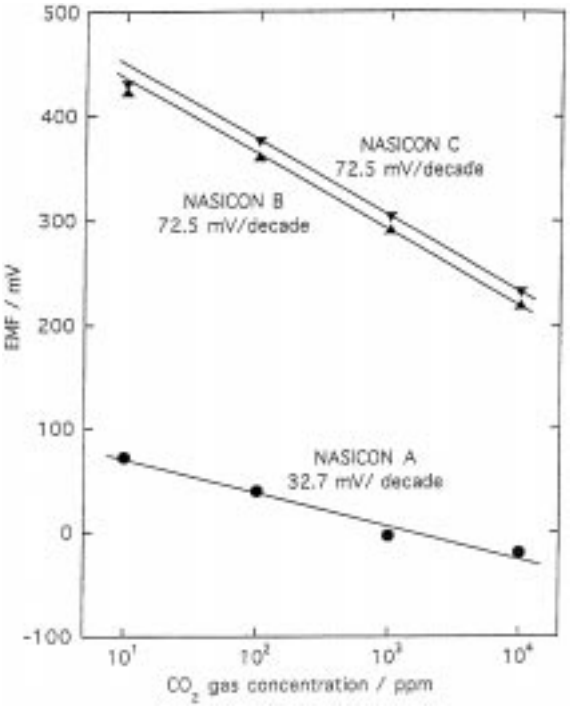

Fig. 9. The CO_2 concentration dependence of the EMF measured at 470°C for the A, B, and C NASICON pellets.

electrochemical gas sensors. This is true even for the C composition, which showed a much lower conductivity. The CO_2 gas sensors using highly dense B and C samples show a stable EMF response, very close to the theoretical value. The strategy of the selection of a proper chemical synthesis for NASICON processing can therefore be of paramount importance to improve the performance of electrochemical devices based on this material.

4. Conclusions

The sol-gel processed NASICON materials are stable along the compositional range $Na_3Zr_{2-(x/4)}Si_{2-x}P_{1+x}O_{12}$, with $0 < x < 1.333$. All the samples within this compositional range showed the presence of a single crystalline phase with rhombohedral symmetry, except for $x = 0$, which is monoclinic. The new sol-gel processed NASICON-type compositions exhibit improved sinterability over the conventional NASICON composition, which improves with increasing x value. This is due to the presence of a glassy phase and occurrence of liquid phase sintering. The high temperature liquid phase, due to its composition, probably allows the growth of only NASICON crystals by a dissolution-reprecipitation mechanism. The conductivity of the samples was affected both by their porosity and lattice parameters. With increasing x, a reduction in conductivity was observed due to the decrease in the tunnel size for fast Na ion migration. Although the conductivity decreased, these dense electrolyte systems are suitable for application as electrochemical gas sensors. The CO_2 gas sensors using highly dense B and C samples show a stable EMF response, very close to the theoretical value.

Acknowledgments

This work was partially supported by the National Research Council of Italy (CNR), under the auspices of the Targeted Project ''Special Materials for Advanced Technologies II'', and partly by Grant-in-Aids for Scientific Research Nos. 1065081 and 10045045 from The Ministry of Education, Science and Culture of Japan.

References

1. M. Gauthier and A. Chamberland, *J. Electrochem. Soc*., **124**, 1579 (1977).
2. G. Hötzel and W. Weppner, *Solid State Ionics*, **18/19**, 1223 (1986).
3. N. Imanaka, T. Kawasato, and G. Adachi, *Chem. Lett*., 497 (1990).
4. S. Yao, Y. Shimizu, N. Miura, and N. Yamazoe, *Chem. Lett*., 2033 (1990).
5. Y. Sadaoka, Y. Sakai, and T. Manabe, *J. Mater. Chem*., **2**, 945 (1992).
6. Y. Sadaoka, Y. Sakai, M. Matsumoto, and T. Manabe, *J. Mater. Sci*., **28**, 5783 (1993).
7. N. Miura, S. Yao, Y. Shimizu, and N. Yamazoe, *Sensors and Actuators B*, **9**, 165 (1992).
8. S. Yao, Y. Shimizu, N. Miura, and N. Yamazoe, *Jpn. J. Appl. Phys*., **31**, (part 2, n. 2B), 197 (1992).
9. N. Miura, S. Yao, Y. Shimizu, and N. Yamazoe, *J. Electrochem. Soc*., **139**, 1384 (1992).
10. O. Bouquin, H. Perthuis, and Ph. Colomban, *J. Mater. Sci. Letters*, **4**, 956 (1985).
11. H.Y-P. Hong, *Mater. Res. Bull*., **11**, 173 (1976).
12. H. Kohler, H. Schulz, and O. Melnikov, *Mater. Res. Bull*., **18**, 1143 (1983).
13. J.P. Boilot, P. Salanié, G. Desplanches, and D. Le Potier, *Mater. Res. Bull*., **14**, 1469 (1979).

14. D.H.H. Quon, T.A. Wheat, and W. Nesbitt, *Mater. Res. Bull.*, **15**, 1533 (1980).
15. G. Desplanches, M. Rigal, and A. Wicker, *Am. Ceram. Soc. Bull.*, **59**, 546 (1980).
16. B.E. Yoldas and I.K. Lloyd, *Mater. Res. Bull.*, **18**, 1171 (1983).
17. A. Caneiro, P. Fabry, H. Khireddine, and E. Siebert, *Analyt. Chem.*, **63**, 2550 (1991).
18. U. Von Alpen, M.F. Bell, R. Brütigan, and H. Laig-Hörstebrock, in *Fast Ion Transport in Solids*, edited by M.V. Vashista, J.N. Mundy, and G.K. Shenoy (North-Holland, Amsterdam, 1979), p. 443.
19. J.W. Hoj and J. Engell, *Mater. Sci. Engineer. B*, **19**, 228 (1993).
20. D. Tran Qui, J.J. Capponi, M. Gondrand, M. Saib, J.C. Joubert, and R.D. Shannon, *Solid State Ionics*, **3/4**, 219 (1981).
21. P.R. Rudolf, M.A. Subramanian, A. Clearfield, and J.D. Jorgensen, *Mater. Res. Bull.*, **20**, 643 (1985).
22. P.R. Rudolf, A. Clearfield, and J.D. Jorgensen, *J. Solid State Chem.*, **72**, 100 (1988).
23. E. Breval and D.K. Agrawal, *Br. Ceram. Trans.*, **94**, 27 (1995).
24. N. Gasmi, N. Gharbi, H. Zarrhouk, P. Barboux, R. Morineau, and J. Livage, *J. Sol-Gel Sci. Technol.*, **4**, 231 (1995).
25. M. Barj, H. Perthuis, and Ph. Colomban, *Solid State Ionics*, **11**, 157 (1983).
26. J.B. Goodenough, H.Y.-P. Hong, and J.A. Kafalas, *Mater. Res. Bull.*, **11**, 203 (1976).
27. U. Von Alpen, M.F. Bell, and W. Wickelhaus, *Mater. Res. Bull.*, **14**, 1317 (1979).
28. A. Ahmad, T.A. Wheat, A.K. Kuriakose, J.D. Canaday, and A.G. McDonald, *Solid State Ionics*, **24**, 89 (1987).
29. U. Von Alpen, M.F. Bell, and H.H. Hofer, *Solid State Ionics*, **3/4**, 215 (1981).
30. A.K. Kuriakose, T.A. Wheat, A. Ahmad, and J. Dirocco, *J. Am. Ceram. Soc.*, **67**, 179 (1984).
31. B.J. McEntire, G.R. Miller, and R.S. Gordon, in *Sintering Processes, Mater. Sci. Res.* Vol. 13, edited by G.C. Kuczynski (Plenum Press, New York, 1979), p. 517.
32. N. Arul Das and K.C. Patil, *J. Mater. Chem.*, **4**, 491 (1994).
33. S. Komarneni, *Int. J. High Tech. Ceram.*, **4**, 31 (1988).
34. G.R. Miller, R.S. Gordon, B.J. McEntire, E.D. Beck, and J.R. Rasmussen, *Solid State Ionics*, **3/4**, 243 (1981).
35. H. Perthuis and Ph. Colomban, *Mater. Res. Bull.*, **19**, 621 (1984).
36. Ph. Colomban and J.P. Boilot, *Rev. Chimie Minérale*, **22**, 235 (1985).
37. H. Perthuis and Ph. Colomban, *Ceram. Intern.*, **12**, 39 (1986).
38. D.K. Agrawal and J.H. Adair, *J. Am. Ceram. Soc.*, **73**, 2153 (1990).
39. J.-H. Choy, Y.-S. Han, Y.-H. Kim, and K.-S. Suh, *Jpn. J. Appl. Phys.*, **32**, 1154 (1993).
40. Ph. Colomban, *Solid State Ionics*, **21**, 97 (1986).
41. J.P. Boilot and Ph. Colomban, in *Sol-gel Technology for Thin Films, Fibers, Preforms, Electronics and Specialty Shapes*, edited by L. Klein (Noyes Publ., 1988), p. 304.
42. Ph. Colomban, *Ceram. Intern.*, **15**, 23 (1989).
43. M.L. Di Vona, S. Licoccia, L. Montanaro, and E. Traversa, *Chem. Mater.*, **11**, 1336 (1999).
44. Y. Shimizu, Y. Azuma, and S. Nichishita, *J. Mater. Chem.*, **7**, 1487 (1997).
45. E. Traversa, L. Montanaro, H. Aono, and Y. Sadaoka, in *Ceram. Trans., Vol. 95*: *Sol-Gel Synthesis and Processing*, edited by S. Komarneni, S. Sakka, P.P. Phule, and R.M. Laine (The Am. Ceram. Soc., Westerville, 1998), p. 225.
46. D. Mazza, M. Lucco Borlera, G. Busca, and A. Delmastro, *J. Europ. Ceram. Soc.*, **11**, 299 (1993).
47. D. Mazza and M. Lucco Borlera, *J. Europ. Ceram. Soc.*, **13**, 61 (1994).
48. L. Montanaro, E. Traversa, A. Negro, M. Lucco Borlera, and D. Mazza, in *Proc. 3rd East Asian Conf. on Chemical Sensors* (Seoul Nat. University, Seoul, 1997), p. 578.
49. C.J. Brinker and G.W. Scherer, *Sol-Gel Science* (Academic Press, San Diego, 1990), p. 109.
50. J.P. Boilot, G. Collin, and Ph. Colomban, in *Progress in Solid Electrolytes* edited by T.A. Wheat, A. Ahmad, and A.K. Kuriakose (ASCOR-CANMET, Ottawa, 1983), p. 91.
51. M. Lucco Borlera, D. Mazza, L. Montanaro, A. Negro, and S. Ronchetti, *Powder Diffraction*, **12**(3), 171 (1997).
52. A. Clearfield, P. Jirustithipong, R.N. Cotman, and S.P. Pack, *Mater. Res. Bull.*, **15**, 1603 (1980).
53. J.P. Boilot, G. Collin, and Ph. Colomban, *J. Solid State Chem.*, **73**, 160 (1988).
54. Ph. Colomban and E. Mouchon, *Solid State Ionics*, **73**, 209 (1994).
55. J.T.S. Irvine, D.C. Sinclair, and A.R. West, *Adv. Mater.*, **2**, 132 (1990).
56. H. Aono and E. Sugimoto, *J. Am. Ceram. Soc.*, **79**, 2786 (1996).
57. K.D. Kreuer, H. Kohler, and J. Maier, in *High Conductivity Ionic Conductors: Recent Trends and Applications*, edited by T. Takahashi (World Scientific Publ., Singapore, 1989), p. 242.
58. H. Aono, E. Sugimoto, Y. Sadaoka, N. Imanaka, and G. Adachi, *Chem. Lett.*, 1825 (1990).
59. H. Aono, E. Sugimoto, Y. Sadaoka, N. Imanaka, and G. Adachi, *J. Electrochem. Soc.*, **140**, 1827 (1993).
60. H. Aono, H. Supriyatno, and Y. Sadaoka, *J. Electrochem. Soc.*, **145**, 2981 (1998).
61. N. Yamazoe and N. Miura, *MRS Bull.*, **24**(6), 37 (1999).